J Mol Model (2012) 18:4453–4464
DOI 10.1007/s00894-012-1449-5

ORIGINAL PAPER

Molecular structure and effects of intermolecular hydrogen bonding on the vibrational spectrum of trifluorothymine, an antitumor and antiviral agent

Çağrı Çırak · Nurettin Koç

Received: 12 March 2012 / Accepted: 25 April 2012 / Published online: 27 May 2012

Abstract In the present work, the experimental and the theoretical vibrational spectra of trifluorothymine were investigated. The FT-IR (400–4000 cm^{-1}) and μ-Raman spectra (100–4000 cm^{-1}) of trifluorothymine in the solid phase were recorded. The geometric parameters (bond lengths and bond angles) and vibrational frequencies of the title molecule in the ground state were calculated using ab initio Hartree–Fock (HF) method and density functional theory (B3LYP) method with the 6-31++G(d, p) and 6-311++G(d,p) basis sets for the first time. The optimized geometric parameters and the theoretical vibrational frequencies were found to be in good agreement with the corresponding experimental data and with results found in the literature. Vibrational frequencies were assigned based on the potential energy distribution using the VEDA 4 program. The dimeric form of trifluorothymine was also simulated to evaluate the effect of intermolecular hydrogen bonding on the vibrational frequencies. It was observed that the stretching modes shifted to lower frequencies, while the in-plane and out-of-plane bending modes shifted to higher frequencies due to the intermolecular N–H···O hydrogen bonds.

Keywords Trifluorothymine · Antitumor agent · FT-IR · Micro-Raman spectroscopy · Hydrogen bonding · Hartree–Fock · DFT

Electronic supplementary material The online version of this article (doi:10.1007/s00894-012-1449-5) contains supplementary material, which is available to authorized users.

Ç. Çırak (✉) · N. Koç
Department of Physics, Arts and Sciences Faculty,
Erzincan University,
24100, Erzincan, Turkey
e-mail: ccirak@erzincan.edu.tr

Introduction

Most pyrimidine derivatives show antitumor, antiviral, antipyretic, and anti-inflammatory activities due to the presence of a pyrimidine base in thymine, cytosine, and uracil, which are the building blocks of DNA and RNA [1]. Because of their biological activities, pyridine-derived biomolecules have received much attention from spectroscopic, clinical, drug, and industrial researchers [1–9].

Fluorinated biomolecules have received attention because, in most cases, they exhibit better bioactivities than their non-fluorinated counterparts [10]. In particular, 5-fluoro-substituted pyrimidines such as 5-fluorouracil, trifluorothymine, ftorafur (tegafur), 5-fluorodeoxyuridine, and so on show significant antitumor activity. Several studies of the synthesis, characterization, and pharmacological applications of fluorinated pyrimidines have been reported in the literature. The properties of fluorine such as its strong electronegativity and small atomic size as well as the low polarizability of the C–F bond can influence the behavior of a fluorine-containing molecule in a biological environment [11]. Introducing fluorine atoms into biomolecules alters their physical, chemical, and biological properties significantly [10, 11]. Furthermore, fluorine is the most abundant halogen in nature, but there are only 13 natural fluorine-containing organic molecules [12]. Therefore, a great deal of effort has been directed into synthesizing fluorine-containing biomolecules due to their biological activities [10, 12].

Trifluorothymine (5-trifluoromethyluracil, 5-trifluoromethyl-1H-pyrimidine-2,4-dione; chemical formula: $C_5H_3F_3N_2O_2$) is a nucleobase that has been modified by adding halogen substituents. Trifluorothymine (TFT) and its derivatives are widely used in antitumor and antiviral agent studies [13–21]. TFT is also synthesized in the human body; Tandon et al. have detected TFT as a metabolite in human urine [20].

An earlier paper [22] reported experimental FT-IR and FT-Raman spectra of 5-trifluoromethyluracil. Experimental single-crystal XRD studies have also been performed on this molecule [2, 23]. To our best knowledge, no computational vibrational study on monomeric and dimeric TFT has been published in the literature. Hence, in the work described in this paper, a theoretical study was performed to obtain a detailed description of the molecular structure and vibrations of TFT, utilizing density functional theory (B3LYP) with the 6-31++G(d,p) and 6-311++G(d,p) basis sets. Experimental FT-IR and μ-Raman spectra of the molecule were also recorded and compared with the results of the theoretical studies.

TFT molecules are interconnected via dimeric N–H···O hydrogen bonds in the solid phase at room temperature [2]. Intermolecular hydrogen bonding between complementary nucleobase pairs is key to the formation of DNA and RNA. However, hydrogen bonding causes significant shifts in the vibrational frequencies of some characteristic modes, so vibrational spectroscopy is very important tool for understanding the effect of hydrogen bonding. Therefore, in this study, we determined the shifts in the vibrational frequencies of dimeric TFT in order to investigate the effects of intermolecular hydrogen bonding in the ground state. Ten et al. have performed studies on the effects of hydrogen bonding on the structure and vibrational spectra of adenine–thymine [24] and adenine–uracil [25] complementary pairs in the ground state. In this study, the effects of hydrogen bonding on vibrational frequencies in the ground state were investigated, but the dynamics of hydrogen bonding in an excited state are very different. Indeed, hydrogen bonding in excited states is particularly important in photophysical processes and photochemical reactions. Excited-state hydrogen-bonding dynamics are mainly determined by the vibrations of the hydrogen donor and acceptor groups [26]. Zhao and Han have made significant contributions to the literature regarding the effect of hydrogen bonding on vibrational spectra in the excited state [27, 28], internal conversion and intersystem crossing [29, 30], and intramolecular charge transfer in the excited state [31].

Experimental details

TFT was purchased from Sigma–Aldrich (St. Louis, MO, USA) and used (i.e., its spectra were recorded) with no further purification. The FT-IR spectrum (400–4000 cm^{-1}) of a KBr disk of TFT was recorded using a PelkinElmer (Waltham, MA, USA) Spectrum One FT-IR spectrometer with a resolution of 4 cm^{-1} at room temperature. The μ-Raman spectrum (100–4000 cm^{-1}) of the title molecule was recorded using a Jasco (Easton, MD, USA) NRS-3100 laser Raman spectrophotometer at room temperature. The 785 nm line of a green diode laser was used as the exciting light, and 25 scans were accumulated.

Computational details

The optimized structure parameters and harmonic vibrational frequencies of TFT were calculated using ab initio Hartree–Fock (HF) method and density functional theory (DFT/B3LYP) method with the 6-31++G(d,p) and 6-311++G(d,p) basis sets. All computations were performed using the Gaussian 03 program package [32]. The calculated harmonic frequencies were scaled by 0.8900 and 0.9600 for the HF and B3LYP levels of theory with the 6-31++G(d,p) basis set [33], and 0.9050 and 0.9614 for the HF and B3LYP levels of theory with the 6-311++G(d,p) basis set [34], respectively. Additionally, the calculated vibrational frequencies were clarified by performing a potential energy distribution (PED) analysis of all the fundamental vibration modes using the VEDA 4 program [35]. VEDA 4 has been used in previous studies by many researchers to realize PED analysis of vibrational modes [36–38].

Results and discussion

The optimized molecular structure of TFT is shown in Fig. 1 along with the atom numbering scheme. As seen in Fig. 1, TFT is a molecule that has 15 atoms. Three Cartesian

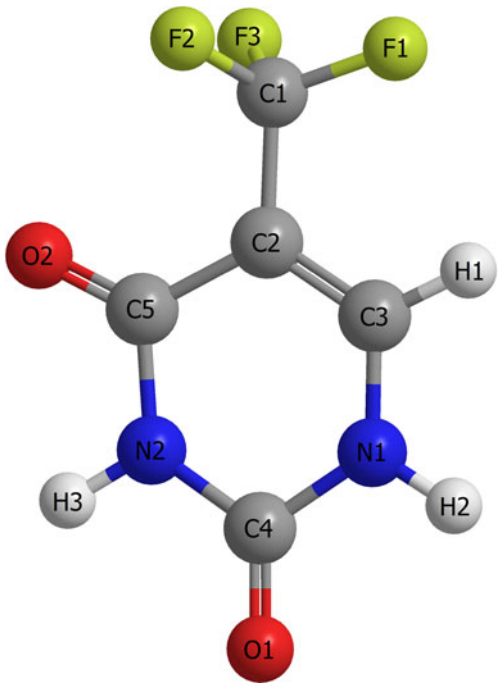

Fig. 1 The optimized molecular structure of TFT

displacements of 15 atoms provide 45 internal and 39 normal vibration modes.

The total energies (corrected for the zero point energy) and the energy differences for the title molecule, calculated using HF and B3LYP with the 6-31++G(d,p) and 6-311++G(d,p) basis sets, are given in Table 1. As clearly shown in Table 1, the geometry optimized using the B3LYP level of theory with the 6-311++G(d,p) basis set has the lowest energy.

Molecular geometry

TFT is a modified thymine where the hydrogen atoms of the methyl group are substituted by fluorine atoms. The crystal structure of the parent molecule, thymine, has been well-characterized (see [39, 40]). Two detailed experimental studies on the crystal structure of TFT have also been performed [2, 23] in the last decade. We have shown the optimized molecular structure of the title molecule in Fig. 1. The optimized geometric parameters (bond lengths and bond angles) obtained using HF and B3LYP with the 6-31++G(d,p) and 6-311++G(d,p) basis sets are presented in Table 2. Graphs comparing the optimized and experimental bond lengths and angles are given in Figs. S1 and S2 of the "Electronic supplementary material" (ESM), respectively. The experimental geometric parameters given in [2, 23] are also tabulated in Table 2 for comparative purposes. As seen from this comparison, the optimized geometric parameters of TFT are in good agreement with the experimental values. The slight differences observed between the calculated and experimental values result from the fact that the theoretical calculations were performed for isolated TFT in the gaseous phase, while the experimental results were obtained for the solid phase of TFT [41]. The largest differences between the calculated (B3LYP/6-311++G(d,p)) and the experimental geometric parameters are: 0.140 Å for the C3–H1 bond, 0.142 Å for the N2–H3 bond, 0.028 Å for the C1–F1 bond, 0.026 Å for the C2–C5 bond, 0.030 Å for the C4–N1 bond, 0.022 Å for the C5=O2 bond, 3.4° for the angle C4–N1–H2, 1.5° for the angle F2–C1–F3, 1.3° for the angle C2–C1–F1, 0.9° for the angle C1–C2–C3, and 0.5° for the angle N2–C5–O2. Also, the calculated bond lengths and angles of the CF_3 group are in good agreement with those reported in the literature [2, 23, 42–44]. The C–F bond lengths of 1.360 Å, 1.347 Å, and 1.347 Å calculated using B3LYP/6-311++G(d,p) are in good agreement with the corresponding experimental values [2, 23]. The C1–C2 (C–CF_3) bond distance of 1.499 Å calculated using B3LYP/6-311++G(d,p) is just 0.018 Å higher than the experimental value of 1.481 Å [23]. The characteristic bond lengths of C4=O1 and C5=O2 were calculated to be 1.209 Å and 1.210 Å, respectively. The corresponding experimental results were 1.232 Å [2] and 1.228 Å [23] for C4=O1, and 1.213 Å [2] and 1.232 Å [23] for C5=O2.

TFT crystallizes in the space group P21/c, and the crystal structure consists of planar thymine molecules linked together by N–H···O hydrogen bonding, with the molecules lined up in a head-to-head fashion [2]. Figure 2 shows the optimized geometry of dimeric TFT. In dimeric TFT, the donor–acceptor (D–A) and hydrogen–acceptor (H···O) distances were calculated to be 2.833 Å (D–A) and 1.811 Å (H···O) for N2–H3···O1' and 2.889 Å (D–A) and 1.873 Å (H···O) for N1'–H2' ···O1, respectively. In the single-crystal XRD spectrum, the D–A and H···O distances were found to be 2.824 Å (D–A) and 1.994 Å (H···O) for N2–H3···O1' and 2.849 Å (D–A) and 2.000 Å (H···O) for N1'–H2'···O1, respectively [2]. As seen from these distance values, the calculated D–A values show very good agreement with recorded spectral data. However, there are small differences between the calculated and experimental hydrogen-bond distances H···O because the calculated N–H bonds are larger than the experimental ones.

Additionally, in order to determine the exact orientation of the CF_3 group, we calculated the total energy for the dihedral angle F1–C1–C2–C5 for θ=120–240° in increments of 10° using the B3LYP level of theory with the 6-311++G(d,p) basis set (Fig. 3). As the curve in Fig. 3 shows, the TFT molecule has its lowest energy when the dihedral angle F1–C1–C2–C5 is 180°. The orientation of the CF_3 group in the most stable form of TFT is also shown in Fig. 3.

Vibrational assignments

To the best of our knowledge, there are no theoretical studies on vibrational assignments for TFT in literature. So, in order to obtain detailed vibrational assignments for TFT, we performed computational analysis. The

Table 1 Calculated total energies and energy differences for TFT

	HF		B3LYP	
	6-31++G(d,p)	6-311++G(d,p)	6-31++G(d,p)	6-311++G(d,p)
Total energy (hartrees)	−748.019738	−748.194899	−751.808680	−751.998527
Energy difference (kcal/mol)	109.9	0.00	119.1	0.0

Table 2 Experimental and calculated geometric parameters of TFT

Geometric parameters	Calculated values				Experimental values	
	HF/6-31++ G(d,p)	B3LYP/6-31++ G(d,p)	HF/6-311++ G(d,p)	B3LYP/6-311++ G(d,p)	Ref [23]	Ref [2]
Bond length (Å)						
C1–C2	1.498	1.500	1.498	1.499	1.481	
C1–F1	1.331	1.364	1.326	1.360	1.332	1.331
C1–F2	1.320	1.351	1.314	1.347	1.331	1.329
C1–F3	1.319	1.351	1.314	1.347	1.350	1.328
C2–C3	1.335	1.356	1.333	1.352	1.346	
C2–C5	1.469	1.469	1.470	1.468	1.442	
C3–H1	1.073	1.084	1.073	1.082	0.940	
C3–N1	1.361	1.366	1.361	1.364	1.353	1.359
C4–N1	1.378	1.399	1.378	1.399	1.369	1.355
C4–N2	1.368	1.382	1.368	1.382	1.370	
C4–O1	1.192	1.217	1.186	1.209	1.228	1.232
C5–N2	1.389	1.410	1.390	1.411	1.380	
C5–O2	1.191	1.218	1.185	1.210	1.232	1.213
N1–H2	0.995	1.011	0.994	1.010	0.870	
N2–H3	0.998	1.015	0.998	1.013	0.870	
Bond angle (°)						
C2–C1–F1	110.4	110.8	110.5	110.9	112.2	111.7
C2–C1–F2	112.3	112.3	112.2	112.3	112.7	113.3
C2–C1–F3	112.3	112.3	112.2	112.3	111.8	112.6
C1–C2–C3	121.5	121.0	121.5	121.0	121.9	121.1
C1–C2–C5	119.3	119.3	119.3	119.3	119.2	119.4
F1–C1–F2	107.0	106.8	107.0	106.8	107.5	107.1
F1–C1–F3	107.0	106.8	107.0	106.8	106.4	105.8
F2–C1–F3	107.5	107.4	107.6	107.4	105.9	105.8
C3–C2–C5	119.1	119.7	119.2	119.7	118.8	119.5
C2–C3–H1	122.1	122.0	122.1	121.9	118.8	
C2–C3–N1	122.2	122.0	122.3	122.1	122.4	121.7
C2–C5–N2	113.7	113.3	113.6	113.1	114.6	113.6
C2–C5–O2	125.5	126.3	125.6	126.3	125.3	126.3
N1–C3–H1	115.7	116.0	115.6	116.0	118.8	
C3–N1–C4	123.4	123.8	123.4	123.8	122.7	122.7
C3–N1–H2	120.9	121.1	120.8	120.9	118.7	
N1–C4–N2	113.7	112.9	113.5	112.7	114.3	115.5
N1–C4–O1	122.4	122.5	122.5	122.6	122.9	122.6
C4–N1–H2	115.7	115.2	115.7	115.2	118.6	
N2–C4–O1	123.8	124.6	123.9	124.7	122.8	121.9
C4–N2–C5	127.8	128.4	128.0	128.6	127.0	127.0
C4–N2–H3	115.9	115.8	115.8	115.7	116.5	120.1
N2–C5–O2	120.7	120.4	120.8	120.6	120.1	
C5–N2–H3	116.3	115.9	116.2	115.7	116.4	

assignments were made using using PED analysis and mode visualization.

Experimental FT-IR and μ-Raman spectra for TFT are shown in Figs. 4 and 5, respectively. The calculated IR and Raman spectra for TFT are shown in Figs. 6 and 7, respectively, for comparative purposes. The scaled harmonic vibrational frequencies calculated for TFT at the HF and B3LYP levels of theory as well as the observed vibrational

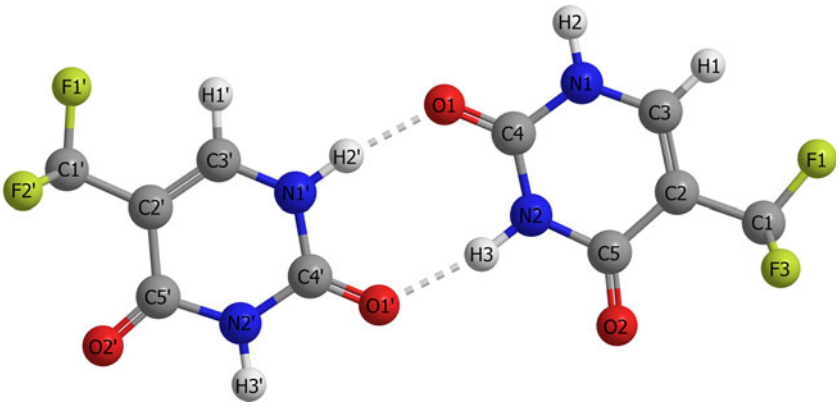

Fig. 2 The optimized molecular structure of dimeric TFT

mode frequencies are presented in Table 3. Table 3 also includes detailed PED assignments and the calculated IR intensities and Raman activities. As seen from Table 3, some bands are not very easy to discern in the experimental spectra due to the presence of intenser broad bands in the same region. A graph comparing the scaled theoretical and experimental vibrational frequencies is given in Fig. S3 of the ESM.

The calculated harmonic frequency values are higher than the observed ones because anharmonicity was not included in the calculations. A scaling procedure was performed to improve the agreement between the harmonic and the observed vibrational frequencies [45]. Also, the harmonic frequencies were calculated for the gaseous phase of isolated TFT, while the experimental spectra were obtained from the solid phase of TFT. TFT molecules are interconnected by dimeric N–H···O hydrogen bonds in the solid phase [2], so the observed and the calculated frequencies do not agree for some modes. However, there is good agreement between the calculated frequencies of monomeric TFT (Fig. 1) and the vibrational spectra of matrix-isolated thymine, uracil, and 1-methyluracil [24, 25, 46]. Therefore, in order to determine the shifts in the normal modes due to the effect of intermolecular hydrogen bonding, we calculated the vibrational frequencies of dimeric TFT as given in [2] using the B3LYP level of theory with the 6-311++G(d,p) basis set. The calculated frequencies of the modes of monomeric TFT that are most strongly affected by intermolecular hydrogen bonding are compared with there corresponding observed frequencies in Table 4. For the modes not shown in Table 4, the average shift to a higher or lower frequency was 5 cm^{-1} . The calculated frequencies and the shift values for dimeric TFT are in good agreement with the theoretical and experimental frequencies for adenine–thymine and adenine–uracil pairs [24, 25].

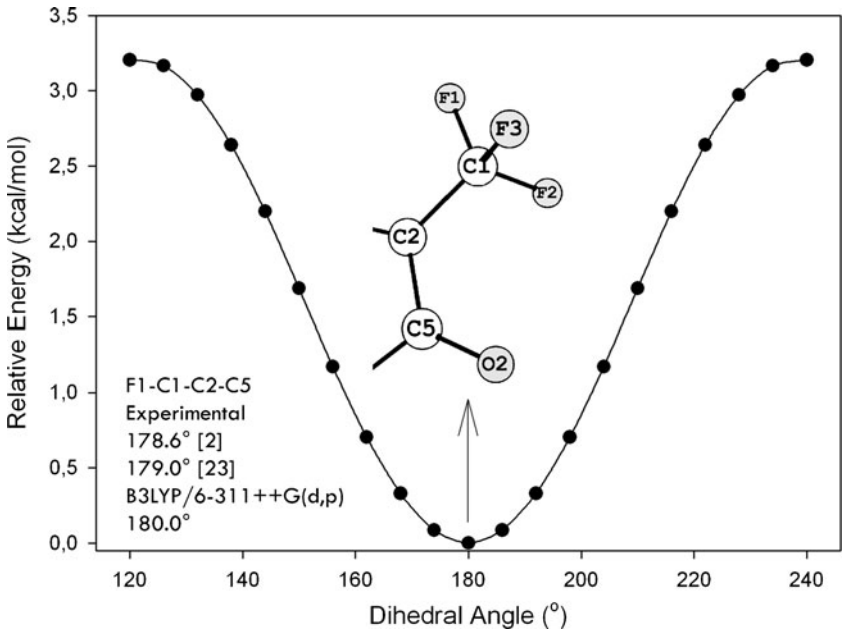

Fig. 3 Energy curve as a function of the dihedral angle F1–C1–C2–C5, and the orientation of the trifluoromethyl group of TFT in the ground state

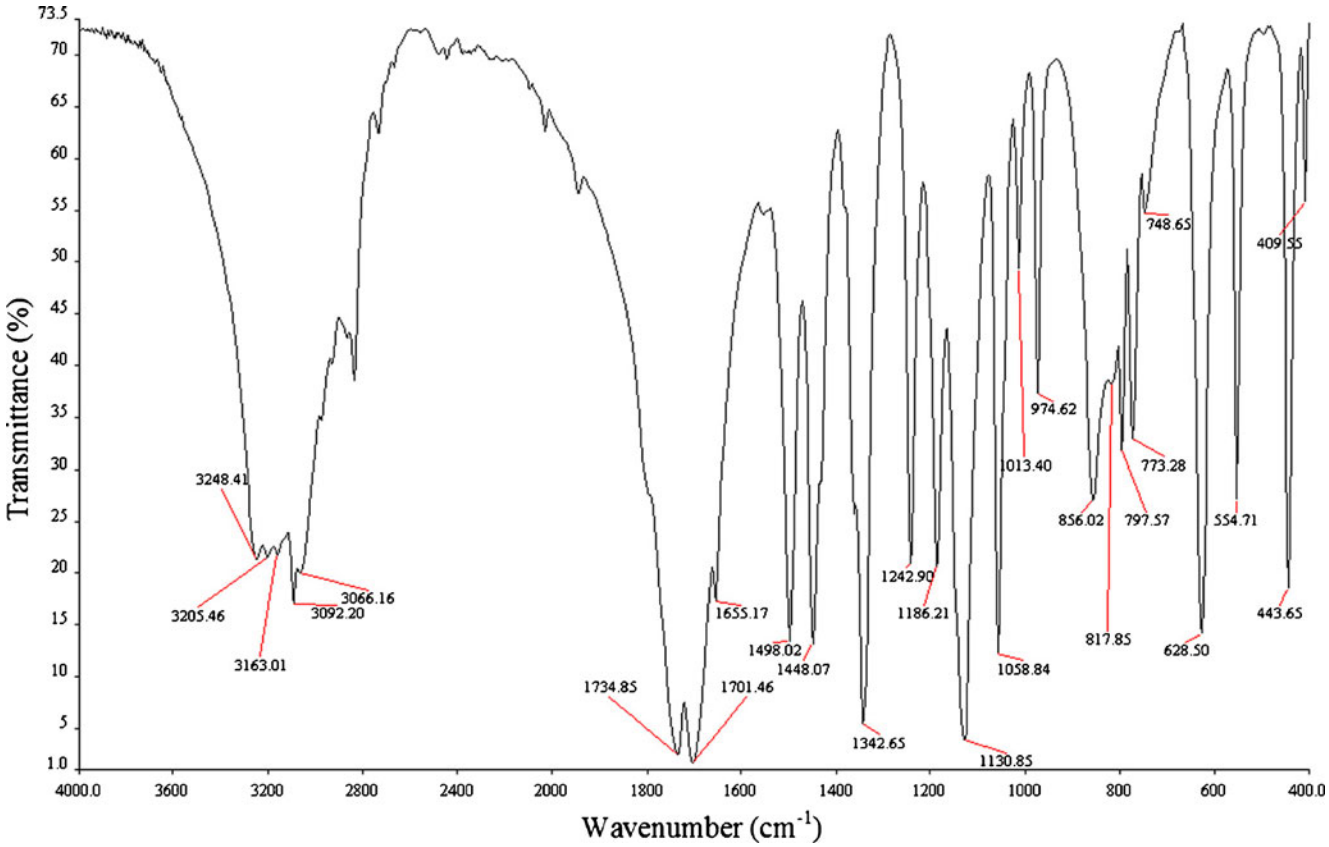

Fig. 4 The experimental FT-IR spectra of TFT in the solid phase

N–H vibrations

In heterocyclic molecules, N–H stretching vibrations are observed in the region 3500–3000 cm^{-1} [47]. As seen in Table 3, two N–H stretching modes are calculated to occur at 3491 and 3456 cm^{-1}, but these modes were not apparent in the experimental spectra. However, Ten et al. did observe these modes at 3479 and 3432 cm^{-1} for isolated thymine [24]. As shown in Table 4, the calculated N1–H2 and N2–H3 stretching modes shifted by 300 cm^{-1} to 3189 and 3155 cm^{-1} in dimeric TFT, respectively. Palafox et al. calculated the N–H stretching modes to occur at 3184 and 3151 cm^{-1} for dimeric 5-aminouracil [48]. These shifted N–H stretching modes were assigned to 3205 (IR) and 3163 (IR) cm^{-1}, respectively, in the experimental spectra, as in [49, 50]. However, no Raman band is observed for the stretching modes of N–H in the experimental spectra.

Based on the results of PED analysis shown in Table 3, N–H in-plane bending (δHNC) vibrations contribute to the four calculated modes at 1449, 1365, 1352, and 1162 cm^{-1}. These frequencies were assigned to 1448 (IR)/1454 (Ra) cm^{-1}, 1362 (IR)/1362 (Ra) cm^{-1}, 1342 (IR)/1338 (Ra) cm^{-1}, and 1160 (Ra) cm^{-1} , respectively, in the experimental FT-IR and μ-Raman spectra shown in Figs. 4 and 5. As seen in Table 4, the N–H in-plane bending modes are shifted by 30–50 cm^{-1} to higher frequencies due to the effect of hydrogen bonding in dimeric TFT. These shifted modes were calculated to occur 1497, 1419, 1383, and 1198 cm^{-1}, and assigned to 1498 (IR)/1492 (Ra), 1419 (Ra), 1390 (IR)/1385 (Ra), and 1186 (IR)/1186 (Ra) cm^{-1}, respectively, in the experimental FT-IR and μ-Raman spectra. The theoretical computed frequencies for N–H in-plane bending vibrations listed in Table 3 and Table 4 show excellent agreement with recorded spectra and results in the literature [3, 22, 24, 25, 48].

The N–H out-of-plane bending vibrations in monomeric TFT were calculated to occur in the region 650–530 cm^{-1}. Three N–H out-of-plane bending vibrations were assigned to 630 (IR)/651 (Ra), 554 (IR)/555 (Ra), and 537 (Ra) cm^{-1} in the experimental spectra. Also, as seen in Table 3, N–H out-of-plane bending vibrations (γHNCC) are observed in the results of PED analysis in three modes. These N–H out-of-plane bending modes were calculated to occur at 643, 561, and 549 cm^{-1}. In dimeric TFT, the calculated N–H out-of-plane bending vibrations were shifted by about 230 cm^{-1} to higher

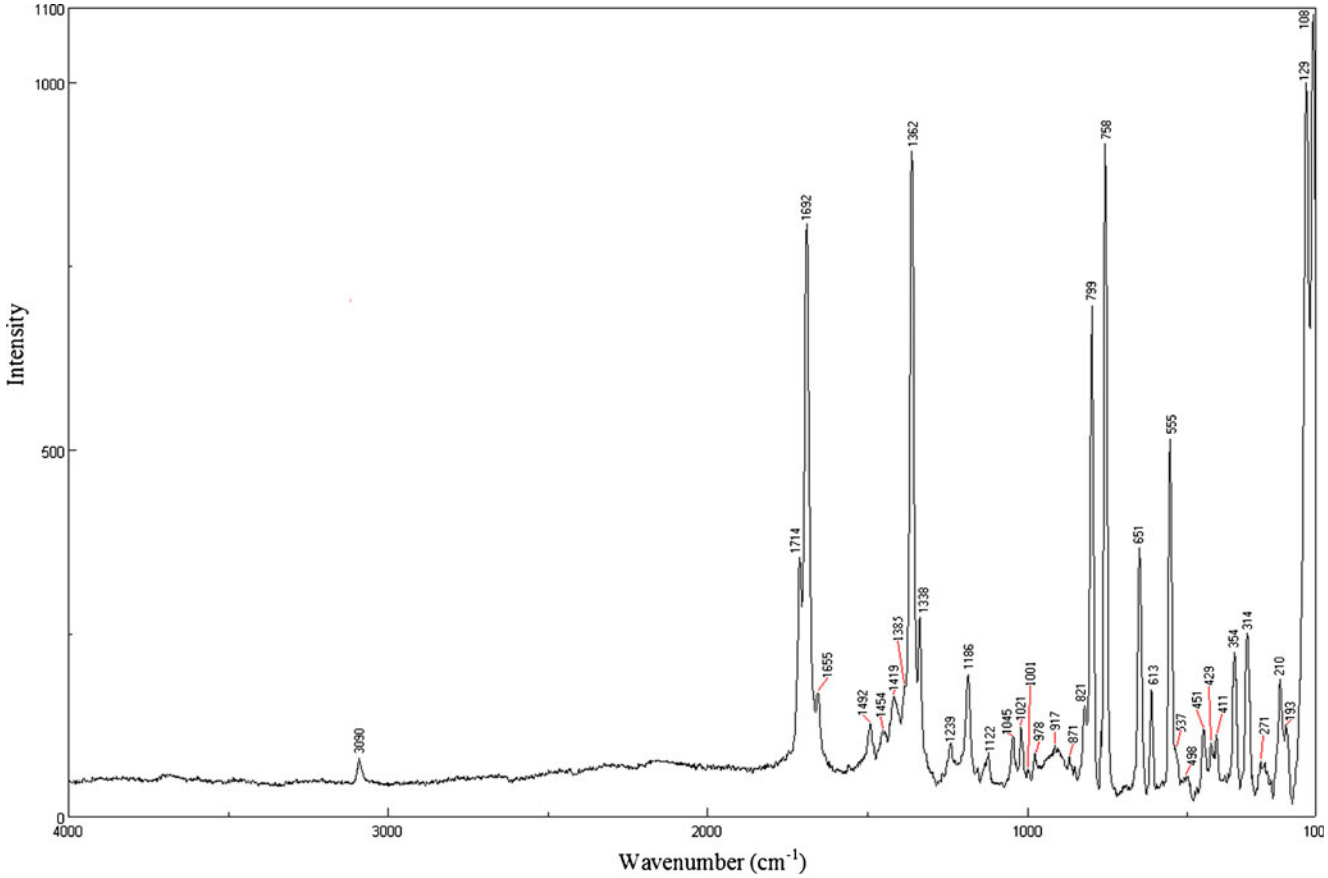

Fig. 5 The experimental μ-Raman spectra of TFT in the solid phase

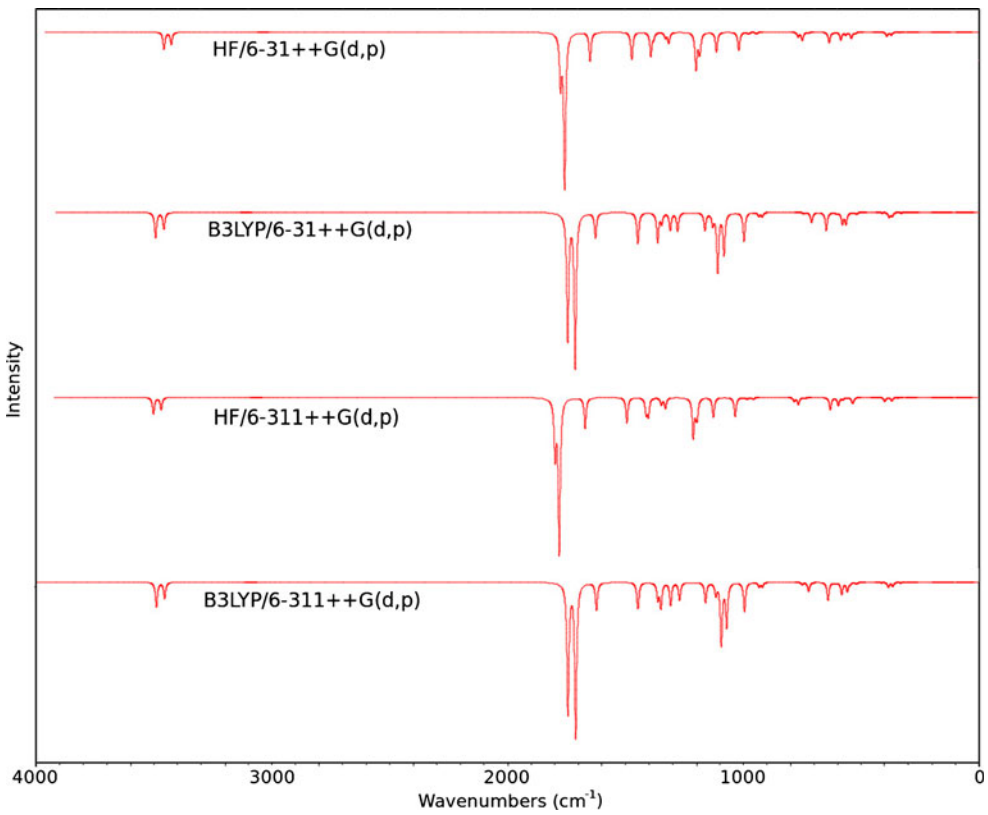

Fig. 6 Graph of the calculated IR spectra

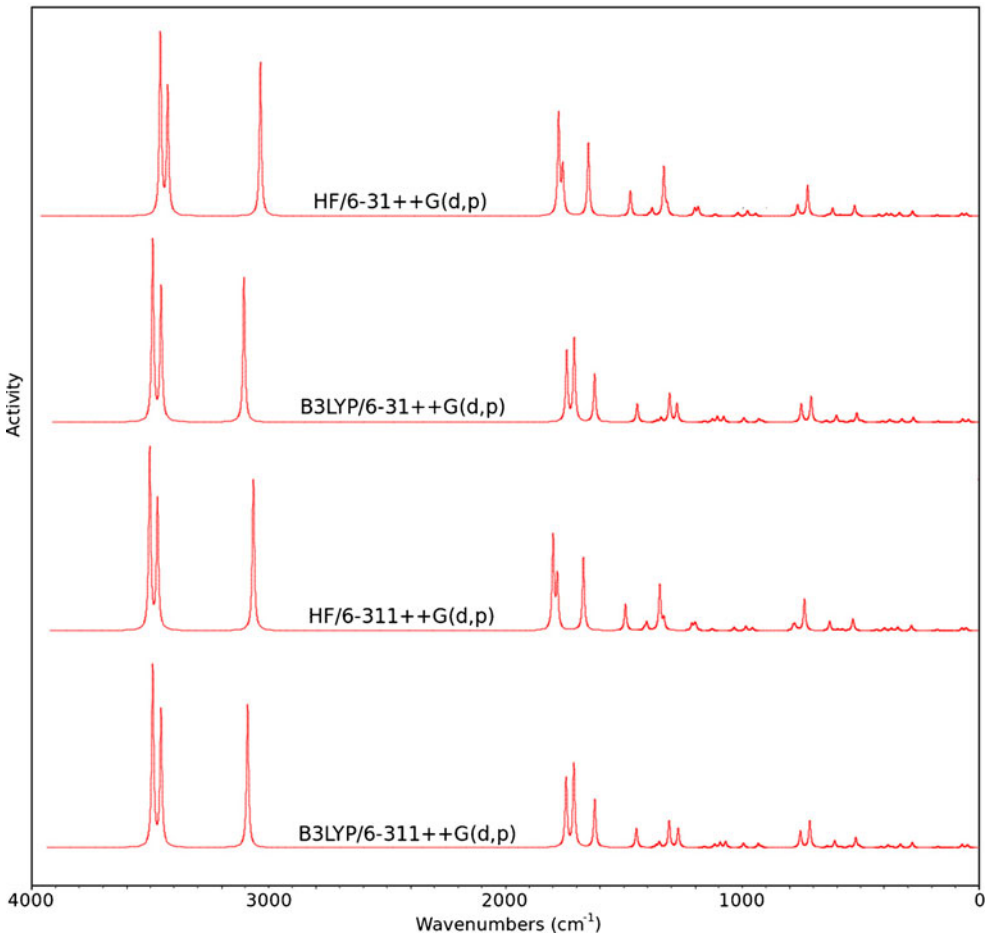

Fig. 7 Graph of calculated Raman spectra

frequencies, 863 and 812 cm^{-1}. This is due to fact that hydrogen-bond formation hampers H atom motion in the direction perpendicular to the N–H bond both in the plane and orthogonal to the plane. This causes out-of-plane bending modes to shift to higher frequencies [25]. We assigned N–H out-of-plane bending modes to the frequencies 857 (IR)/869 (Ra) and 818 (IR)/821 (Ra) in the experimental spectra, as in [22, 50].

C–H vibrations

In heterocyclic organic molecules, C–H stretching modes are observed commonly in the region 3100–3000 cm^{-1} [45]. Table 3 lists a calculated C–H stretching mode that occurs at 3090 cm^{-1}. From the experimental FT-IR and μ-Raman spectra given in Figs. 4 and 5, the observed peaks at 3092 (IR)/3090 (Ra) were assigned to a C–H stretching mode of TFT. As seen from the results of PED analysis in Table 3, C–H in-plane bending vibrations (δHCC) contribute to some modes in the region 1600–1100 cm^{-1}. Hence, an FT-IR band at 1362 cm^{-1} and μ-Raman bands at 1362 and 1160 cm^{-1} were assigned to C–H in-plane bending. The calculated mode at 921 cm^{-1} given in Table 3 was assigned to the C–H out-of-plane bending mode at 917 cm^{-1} in the μ-Raman spectrum.

C=O vibrations

Typical characteristic absorption bands of C=O stretching vibrations of uracil and its derivatives are very complex, and appear as very broad and strong IR bands [51]. At first glance, the observed bands at 1734 (IR)/1714 (Ra) cm^{-1} and 1701 (IR)/1692 (Ra) cm^{-1} can be assigned to C4=O1 and C5=O2 stretching modes, respectively. However, the C4=O1 stretching mode was calculated to occur at a lower frequency than the C5=O2 mode in dimeric TFT. The crystal structure consists of TFT molecules linked by dimeric N–H···O hydrogen bonds involving N1, N2, and the keto oxygen O1 [2]. O2 is not involved in this N–H···O hydrogen bond. As seen from Table 4, the C4=O1 stretching-mode frequency changes noticeably due to hydrogen bonding. This frequency was calculated to be 1746 cm^{-1} in monomeric TFT (Table 3), but it is shifted by 45 cm^{-1} to the lower frequency of 1701 cm^{-1} in dimeric TFT (Table 4), while the C5=O2 stretching mode was calculated to occur at 1713 and

Table 3 Observed and calculated vibrational frequencies of TFT

Vibration no.	Calculated frequencies in cm^{-1} (IR intensity/Raman activity)		Calculated frequencies in cm^{-1} (IR intensity/Raman activity)		Observed frequencies		Assigments
	HF/6-31++G(d,p)	B3LYP/6-31++G(d,p)	HF/6-311++G(d,p)	B3LYP/6-311++ G(d,p)	FT-IR	μ-Raman	
ν1	3459 (154.7/78.4)	3495 (125.2/102.8)	3504 (149.3/77.7)	3491 (123.6/100.4)			νNH(100)
ν2	3428 (113.4/55.0)	3459 (81.2/76.0)	3471 (108.6/55.8)	3456 (79.9/75.6)			νNH(100)
ν3	3036 (0.8/66.5)	3109 (0.9/82.4)	3066 (0.7/64.6)	3090 (1.0/79.2)	3092 s	3090 w	νCH(99)
ν4	1777 (456.3/43.9)	1747 (630.6/40.0)	1801 (500.8/40.1)	1746 (650.6/38.1)	1735 vs	1714 s	νOC(80)
ν5	1760 (1406.8/20.1)	1715 (766.1/47.2)	1783 (1396.4/22.4)	1713 (769.5/46.0)	1701 vs	1692 vs	νOC(79)
ν6	1652 (264.4/31.6)	1629 (125.1/27.3)	1673 (270.9/31.2)	1625 (137.3/26.8)	1655 s	1655 m	νCC(63)+δHCC(13)
ν7	1474 (249.9/10.9)	1449 (153.5/10.3)	1495 (225.9/11.3)	1449 (132.4/10.6)	1448 s	1454 m	δCCN(56)+νNC(22)
ν8	1395 (216.2/0.9)	1366 (147.6/0.9)	1415 (138.9/1.2)	1365 (81.5/1.1)	1362 sh	1362 vs	δHNC(41)+νOC(13)+δHCC(10)
ν9	1383 (45.0/3.3)	1348 (50.1/2.5)	1405 (153.8/3.4)	1352 (124.0/3.1)	1343 vs	1338 m	δHNC(38)+νNC(23)+δOCN(12)
ν10	1333 (47.8/21.3)	1312 (86.1/16.1)	1350 (62.2/19.6)	1311 (112.7/14.7)	1343 vs	1338 m	δHCC(44)+νCC(17)+νNC(12)
ν11	1319 (98.0/3.6)	1281 (91.6/10.3)	1333 (95.2/4.7)	1273 (88.3/10.5)	1243 s	1239 w	νCC(33)+νNC(16)+δFCF(13)+ νFC(12)
ν12	1203 (332.3/3.2)	1165 (87.7/0.7)	1215 (351.0/2.9)	1162 (100.0/0.6)	1186 s	1186 m	νNC(25)+δHCC(19)+νHNC(18)
ν13	1189 (121.0/3.1)	1132 (56.3/1.7)	1203 (97.8/2.3)	1119 (57.9/1.8)	1131vs	1122 w	νNC(51)+νFC(10)
ν14	1185 (94.2/0.9)	1111 (293.2/3.3)	1197 (138.9/1.8)	1095 (308.3/2.9)	1059 s	1045 w	νFC(77)+γFCFC(12)
ν15	1116 (180.5/0.9)	1084 (206.5/3.1)	1129 (177.2/0.9)	1072 (216.6/3.3)	1059 s	1045 w	νFC(54)+νNC(12)
ν16	1021 (168.6/1.5)	999 (144.4/2.6)	1036 (174.0/1.4)	997 (145.9/2.5)	1013 m	1021 m	νFC(29)+δCCN(20)
ν17	980 (16.8/2.3)	935 (18.0/2.0)	986 (15.8/1.9)	934 (23.3/2.2)		917 w	δCNC(28)+νNC(27)+δOCN(10)
ν18	946 (16.4/1.1)	921 (20.7/0.9)	959 (17.7/1.2)	921 (21.1/0.6)		917 w	γHCCC(83)
ν19	770 (39.6/1.9)	757 (0.5/10.2)	787 (32.9/1.9)	756 (0.4/8.8)	749 m	758 vs	νNC(33)+δCNC(17)+νFC(12)+ δNCN(11)
ν20	767 (1.3/3.2)	746 (5.6/0.6)	780 (0.6/2.2)	752 (10.9/0.6)	749 m	758 vs	νOC(79)+γONNC(78)
ν21	752 (74.2/0.4)	715 (1.3/14.7)	769 (62.9/0.5)	725 (45.4/0.1)			γONNC(87)
ν22	726 (6.6/13.5)	713 (48.5/0.1)	739 (8.2/13.5)	717 (1.4/14.8)			νFC(34)+δFCF(18)+νNC(13)+ δNCN(11)
ν23	638 (97.5/0.6)	650 (89.5/0.8)	634 (105.4/0.5)	643 (89.2/0.7)	629 s	651 s	γHNCC(89)
ν24	620 (4.2/3.4)	608 (4.6/3.9)	633 (4.4/3.4)	611 (5.2/3.9)		613 m	δOCN(42)+νFC(12)+δCCC(12)
ν25	589 (71.3/0.5)	582 (58.0/0.4)	599 (72.0/0.6)	585 (58.8/0.4)			δNCN(37)+δFCF(28)+δCNC(13)
ν26	568 (23.1/0.4)	567 (56.2/0.1)	580 (18.8/0.6)	561 (44.4/0.1)	555 s	555 s	γHNCC(66)+γFCFC(16)
ν27	544 (55.3/0.1)	547 (0.4/0.7)	539 (49.5/0.1)	549 (7.7/0.8)		537 sh	γHNCC(32)+γFCFC(24)+ νFC(11)+δFCF(10)
ν28	527 (11.3/4.5)	522 (8.6/5.4)	535 (10.6/4.7)	523 (8.7/5.5)		537 sh	δCNC(43)+νNC(26)
ν29	515 (0.2/0.4)	501 (0.5/0.7)	529 (1.0/0.4)	507 (0.7/0.8)	497 w	498 w	δFCF(45)+δOCN(18)+ γFCFC(15)+νFC(11)
ν30	426 (1.9/0.6)	414 (3.0/0.6)	435 (1.4/0.5)	416 (2.5/0.5)		429 w	δFCF(55)+γCCCC(16)
ν31	393 (36.1/1.2)	383 (24.8/1.5)	402 (35.5/1.1)	386 (24.3/1.5)	410 m	411 m	δOCN(49)+δCNC(20)
ν32	374 (27.3/0.9)	370 (18.7/0.4)	372 (31.7/1.0)	368 (20.8/0.4)		354 m	τCCNC(55)+τCNCN(13)
ν33	338 (4.7/1.5)	332 (3.4/1.8)	346 (4.4/1.5)	334 (3.3/1.8)		314 m	δFCF(32)+γFCFC(21)
ν34	283 (0.5/2.1)	283 (0.3/2.7)	288 (0.5/2.2)	284 (0.3/2.8)		271 w	νCC(28)+δCCN(13)+δFCF (13)
ν35	179 (0.1/0.5)	179 (0.2/0.5)	178 (0.1/0.6)	176 (0.1/0.6)		193 m	γCCCC(35)+τCNCN(22)+ γFCFC(14)
ν36	157 (1.3/0.1)	158 (1.2/0.1)	160 (1.4/0.1)	159 (1.2/0.1)		129 vs	δCCC(58)+δCCN(11)+ γFCFC(11)
ν37	145 (1.1/0.1)	142 (1.2/0.1)	136 (0.7/0.1)	134 (1.1/0.1)			τCNCN(85)
ν38	75 (2.9/1.1)	75 (2.9/1.8)	75 (2.8/1.1)	74 (2.8/1.7)			τCNCN(49)+τCCNC(26)
ν39	56 (0.5/1.2)	50 (0.4/1.5)	57 (0.5/1.2)	50 (0.4/1.5)			τFCCC(75)+γCCCC(15)

ν stretching, δ in-plane bending, γ out-of-plane bending, τ torsion, *vs* very strong, *s* strong, *m* medium, *w* weak

PED values lower than 10% are neglected

Table 4 Observed and calculated vibrational frequencies of TFT calculated at the B3LYP/6-311++G(d,p) level of theory

Vibration no.	Calculated frequencies in cm^{-1} (IR intensity/Raman activity)		Shift values (cm^{-1})	Observed frequencies		Mode assignments
	Monomeric	Dimeric		FT-IR	μ-Raman	
ν1	3491 (123.6/100.4)	3189 (2553.2/18.3)	302	3205 s		ν(N1–H2)
ν2	3456 (79.9/75.6)	3155 (0.9/725.5)	301	3163 s		ν(N2–H3)
ν4	1746 (650.6/38.1)	1692 (734.3/36.1)	54	1701 vs	1692vs	ν(C4=O2)
ν7	1449 (132.4/10.6)	1497 (95.6/45.3)	−48	1498 s	1492 m	δ(N1–H2)
ν8	1365 (81.5/1.1)	1419 (13.3/24.7)	−54		1419 m	δ(N2–H3)
ν9	1352 (124.0/3.1)	1383 (235.7/4.4)	−32	1390 sh	1385sh	δ(N1–H2)+$\nu(C–N)_{asym}$
ν12	1162 (100.0/0.6)	1198 (140.4/1.9)	−36	1186 m	1186 m	δ(N1–H2)+δ(C3–H1)
ν17	934 (23.3/2.2)	959 (13.5/2.2)	−25	975 m	978w	angle deformation(C4–N1–C3)
ν23	643 (89.2/0.7)	863 (148.9/1.3)	−220	857 m	869w	γ(N2–H3)
ν25	561 (44.4/0.1)	812 (16.9/0.4)	−251	818 sh	821 m	γ(N1–H2)
ν31	386 (24.3/1.5)	411 (87.2/2.7)	−25	410 m	411w	δ(C4=O1)
		113 (0.3/0.5)				Lattice mode
		54 (0.5/0.1)				Lattice mode
		42 (1.3/0.4)				Lattice mode

ν stretching, δ in-plane bending, γ out-of-plane bending, τ torsion, *vs* very strong, *s* strong, *m* medium, *w* weak

1720 cm^{-1} in monomeric and dimeric TFT, respectively. For this reason, we believe that observed bands at 1734 (IR)/1714 (Ra) cm^{-1} and 1701 (IR)/1692 (Ra)cm^{-1} should be assigned to the C5=O2 and C4=O1 stretching modes, respectively. Furthermore, the observed bands at 410 (IR)/411 (Ra) were assigned to C=O in-plane bending vibrations, while the observed bands at 752 (IR)/758 (Ra) cm^{-1} were assigned to C=O out-of-plane bending. The calculated and experimental C=O vibrational frequencies show excellent agreement with those seen in our recent study of 5-bromo-2′-deoxyuridine [3].

CF_3/C–CF_3 vibrations

The assignments for the fluoromethyl group vibrations of TFT and various molecules are discussed in the literature [22, 42–44]. Our assignments, shown in Table 3, are in good agreement with the results of previous studies. As seen from the results of PED analysis in Table 3, CF_3 group vibrations contribute to many frequencies in the fingerprint region. In the mid-IR region, the bands observed at 1130 (IR)/1122 (Ra) cm^{-1}, 1058 (IR)/1045 (Ra) cm^{-1}, and 1013 (IR)/1021 (Ra) cm^{-1} were assigned to C–F stretching modes. CF_3 group deformation vibrations were identified in the region 720–300 cm^{-1} [22, 42–44]. However, some bands were not observed in the experimental spectra due to the presence of intenser broad bands located in the same region. Bands observed at 497 (IR) cm^{-1} 429 (Ra) cm^{-1}, and 314 (Ra) cm^{-1} were assigned to FCF angle deformation modes. Also, bands at 1242 (IR)/1239 (Ra) cm^{-1} were assigned to C–CF_3 stretching, while those at 193 (Ra) cm^{-1} and 130 (Ra) cm^{-1} were assigned to C–CF_3 out-of-plane bending and in-plane bending vibrations, respectively.

Conclusion

In this work, we performed experimental and theoretical vibrational analysis, and investigated the structural geometry of the TFT molecule. Calculations were performed at the HF and B3LYP levels of theory with the 6-31++G(d,p) and 6-311++G(d,p) basis sets. Based on the calculated energies, the optimized structure at the B3LYP/6-311++G(d,p) level of theory had the lowest energy. The parameters of the optimized structure were also in good agreement with the results of previous experimental studies. The scaled harmonic vibrational frequencies were compared with those observed in recorded FT-IR and μ-Raman spectra, and quite good agreement between the observed and the calculated frequencies was noted. Also, the results of our detailed PED analysis were in good agreement with results reported in the literature and the theoretical background. Vibrational analysis of the dimeric TFT molecule enabled us to evaluate the effect of hydrogen bonding on the vibrational frequencies and to improve the accuracy of assignments to the experimental spectra. Calculations performed at the B3LYP/6-311++G(d,p) level yielded good results for TFT in terms of calculated frequencies and optimized geometric parameters.

Acknowledgements This work was supported by the research fund of Erzincan University (project no: 2011BAP-10.01.15). The computing resources used in this work were provided by the National Center for High Performance Computing of Turkey (UYBHM) under grant number 10812009. We also thank Assist. Prof. Dr. Hamit Mermerkaya for his assistance.

References

1. Amir M, Javed SA, Kumar H (2007) Pyrimidine as antiinflammatory agent: a review. Indian J Pharm Sci 69:337–343
2. Rajeswaran M, Srikrishnan T (2008) Crystal and molecular structure of 5-trifluorothymine, a metabolite from human urine: role of fluorine in stacking and hydrogen bonded interactions. J Fluor Chem 129:493–497
3. Çırak Ç, Sert Y, Ucun F (2012) Experimental and computational study on molecular structure and vibrational analysis of a modified biomolecule: 5-bromo-2′-deoxyuridine. Spectrochim Acta A 92:406–414
4. Aruna S, Shanmugam G (1985) Vibrational assignments of six-membered heterocyclic compounds: normal vibrations of 6-amino uracil and 6-amino 2-thiouracil. Spectrochim Acta A 41:531–536
5. Bandekar J, Zundel G (1983) Normal coordinate analysis treatment on uracil in solid state. Spectrochim Acta A 39:343–355
6. Demirbaş N, Uğurluoğlu R, Demirbaş (2002) Synthesis of 3-alkyl (aryl)-4-alkylidenamino-4,5-dihydro-1H-1,2,4-triazol-5-ones and 3-alkyl-4-alkylamino-4,5-dihydro-1H-1,2,4-triazol-5-ones as antitumor agents. Bioorg Med Chem 10:3717–3723
7. Emilsson H, Selander H, Gaarder J (1985) Synthesis and antihypertensive activity of 3-amino-4-(arylideneamino)-4H-1,2,4-triazoles. Eur J Med Chem 20:333–337
8. Swarup S, Saxena VK (1991) Synthesis and pharmacological screening of some new 1-phenyl-3-(4-substituted-phenoxy-phenyl)-5-substituted-benzylidino)thiobarbituric acids. J Indian Chem Soc 68:302–304
9. Rastogi VK, Mittal HP, Sharma YC, Sharma SN (1991) Spectroscopy of biological molecules. Royal Society of Chemistry, London, 403–404
10. Qiu XL, Qing FL (2011) Recent advances in the synthesis of fluorinated amino acids. Eur J Org Chem 2011:3261–3278
11. Oh CH, Hong JH (2007) Short synthesis and antiviral evaluation of C-fluoro-branched cyclopropyl nucleosides. Nucleosides Nucleotides Nucleic Acids 26:403–411
12. O'Hagan D, Harper DB (1999) Fluorine-containing natural products. J Fluor Chem 100:127–133
13. Umeda M, Heidelberger C (1968) Comparative studies of fluorinated pyrimidines with various cell lines. Cancer Res 28:2529–2538
14. Yamashita J, Yasumoto M, Takeda S, Matsumoto H, Unemi NJ (1989) Studies on antitumor agents. 8. Antitumor activities of O-alkyl derivatives of 2′-deoxy-5-(trifluoromethyl)uridine and 2′-deoxy-5-fluorouridine. J Med Chem 32:136–139
15. Kaufman HE, Heidelberger C (1964) Therapeutic antiviral action of 5-trifluoromethyl-2-deoxyuridine in Herpes simplex keratitis. Science 145:585–586
16. Wingard JR, Stuart RK, Saral R, Burns WH (1981) Activity of trifluorothymidine against cytomegalovirus. Antimicrob Agents Chemother 20:286–290
17. Carmine AA, Brogden RN, Heel RC, Speight TM, Avery GS (1982) Trifluridine: a review of its antiviral activity and therapeutic use in the topical treatment of viral eye infections. Drugs 23:329–353
18. Srivastav NC, Mak M, Agrawal B, Tyrrell DLJ, Kumar R (2010) Antiviral activity of 2,3-anhydro and related pyrimidine nucleosides against hepatitis B virus. Bioorg Med Chem Lett 20:6790–6793
19. Srivastav NC, Shakya N, Mak M, Agrawal B, Tyrrell DL, Kumar R (2010) Antiviral activity of various 1-(2-deoxy-β-D-lyxofuranosyl), 1-(2-fluoro-β-D-xylofuranosyl), 1-(3-fluoro-β-D-arabinofuranosyl), and 2-fluoro-2,3-didehydro-2,3′-dideoxyribose pyrimidine nucleoside analogues against duck hepatitis B virus (DHBV) and human hepatitis B virus (HBV) replication. J Med Chem 53:7156–7166
20. Tandon M, Kumar P, Wiebe G, Wiebe LI (1992) Detection of new metabolites of trifluridine (F3TdR) using 19F NMR spectroscopy. Biochem Pharmacol 44:2223–2228
21. Benci K, Wittine K, Radan M, Cetina M, Sedić M, Kraljević Pavelić S, Pavelić K, Clercq ED, Mintas M (2010) The unsaturated acyclic nucleoside analogues bearing a sterically constrained (*Z*)-4-benzamido-2-butenyl moiety: synthesis, X-ray crystal structure study, cytostatic and antiviral activity evaluations. Bioorg Med Chem 18:6249–6257
22. Shanker R, Yadav RA, Singh IS (1994) Vibrational studies, barrier height and thermodynamic functions for biomolecules: 5-trifluoromethyl uracil. Spectrochim Acta A 50:1251–1258
23. Twamley B, Gupta OD, Shreeve JM (2002) 5-(Trifluoromethyl) uracil. Acta Crystallogr E 58:1040–1042
24. Ten GN, Nechaev VV, Pankratov AN, Berezin VI, Baranov VI (2010) Effect of hydrogen bonding on the structure and vibrational spectra of the complementary pairs of nucleic acid bases. J Struct Chem 51:854–861
25. Ten GN, Nechaev VV, Pankratov AN, Baranov VI (2010) Hydrogen bonding effect on the structure and vibrational spectra of complementary pairs of nucleic acid bases. I. Adenine–uracil. J Struct Chem 51:453–462
26. Zhao GJ, Han KL (2012) Hydrogen bonding in the electronic excited state. Acc Chem Res 45:404–413
27. Zhao GJ, Han KL (2007) Early time hydrogen-bonding dynamics of photoexcited coumarin 102 in hydrogen-donating solvents: theoretical study. J Phys Chem A 11:2469–2474
28. Zhao GJ, Han KL (2008) Effects of hydrogen bonding on tuning photochemistry: concerted hydrogen-bond strengthening and weakening. ChemPhysChem 9:1842–1846
29. Zhao GJ, Han KL (2007) Ultrafast hydrogen bond strengthening of the photoexcited fluorenone in alcohols for facilitating the fluorescence quenching. J Phys Chem 111:9218–9223
30. Zhao GJ, Han KL (2009) Role of intramolecular and intermolecular hydrogen bonding in both singlet and triplet excited states of aminofluorenones on internal conversion, intersystem crossing, and twisted intramolecular charge transfer. J Phys Chem A 113:14329–14335
31. Zhao GJ, Han KL (2008) Time-dependent density functional theory study on hydrogen-bonded intramolecular charge-transfer excited state of 4-dimethylamino-benzonitrile in methanol. J Comput Chem 29:2010–2017
32. Frisch MJ, Trucks GW, Schlegel HB, Scuseria GE, Robb MA, Cheeseman JR, Montgomery JA, Vreven T, Kudin KN, Burant JC, Millam JM, Iyengar SS, Tomasi J, Barone V, Mennucci B, Cossi M, Scalmani G, Rega N, Petersson GA, Nakatsuji H, Hada M, Ehara M, Toyota K, Fukuda R, Hasegawa J, Ishida M, Nakajima T, Honda Y, Kitao O, Nakai H, Klene M, Li X, Knox JE, Hratchian HP, Cross JB, Bakken V, Adamo C, Jaramillo J, Gomperts R, Stratmann RE, Yazyev O, Austin AJ, Cammi R, Pomelli C, Ochterski JW, Ayala PY, Morokuma K, Voth GA, Salvador P, Dannenberg JJ, Zakrzewski VG, Dapprich S, Daniels AD, Strain MC, Farkas O, Malick DK, Rabuck AD, Raghavachari K, Foresman JB, Ortiz JV, Cui Q, Baboul AG, Clifford S, Cioslowski J, Stefanov BB, Liu G,Liashenko A, Piskorz P, Komaromi I, Martin RL, Fox DJ, Keith T, Al- Laham MA, Peng CY,Nanayakkara A, Challacombe M, Gill PMW, Johnson B, Chen W, Wong MW, Gonzalez C, Pople J (2004) Gaussian 03, revision D.01. Wallingford, CT

33. Pekparlak A, Avcı D, Cömert H, Atalay Y (2010) Theoretical studies of molecular structure and vibrational spectra of melaminium acetate acetic acid solvate monohydrate. Spectrochim Acta A 77:696–702
34. Young DC (2001) Computational chemistry: a practical guide for applying techniques to real-world problems. Wiley, New York
35. Jamróz MH (2004) Vibrational energy distribution analysis, VEDA 4. M.H. Jamróz, Warsaw
36. Jamróz MH, Dobrowolski JC, Brzozowski R (2006) Vibrational modes of 2,6-, 2,7-, and 2,3-diisopropylnaphthalene. A DFT study. J Mol Struct 787:172–183
37. Çırak Ç, Demir S, Ucun F, Çubuk O (2011) Experimental and theoretical study on the structure and vibrational spectra of β-2-aminopyridinium dihydrogenphosphate. Spectrochim Acta A 79:529–532
38. Arslan H, Algül Ö, Dündar Y (2007) Structural and spectral studies on 3-(6-benzoyl-5-chloro-2-benzoxazolinon-3-yl) propanoic acid. Vib Spectrosc 44:248–255
39. Ozeki K, Sakabe N, Tanaka J (1969) The crystal structure of thymine. Acta Crystallogr B 25:1038–1045
40. Portalone G, Bencivenni L, Colapietro M, Pieretti A, Ramondo F (1999) The effect of hydrogen bonding on the structures of uracil and some methyl derivatives studied by experiment and theory. Acta Chem Scand 53:57–68
41. Sundaraganesan N, Kalaichelvan S, Meganathan C, Joshua BD, Cornard J (2008) FT-IR, FT-Raman spectra and ab initio HF and DFT calculations of 4-*N*,*N*-dimethylamino pyridine. Spectrochim Acta A 71:898–906
42. Balci K, Akkaya Y, Akyuz S (2010) An experimental and theoretical vibrational spectroscopic study on niflumic acid, a non-steroidal anti-inflammatory drug. Vib Spectrosc 53:239–247
43. Álvarez RMS, Cutin EH, Romano RM, Della Védova CO (1999) Vibrational spectra and theoretical calculations of *N*-(trifluoromethyl) iminosulphur dichloride: CF3N=SCl2. Spectrochim Acta A 55:2615–2622
44. Sert Y, Ucun F, Böyükata M (2008) Conformational and vibrational analysis of 2-, 3- and 4-trifluoromethylbenzaldehyde by ab initio Hartree–Fock, density functional theory and Moller–Plesset pertubation theory calculations. J Mol Struct (THEOCHEM) 861:122–130
45. Ramalingam S, Periandy S, Mohan S (2010) Vibrational spectroscopy (FTIR and FT-Raman) investigation using ab initio (HF) and DFT (B3LYP and B3PW91) analysis on the structure of 2-amino pyridine. Spectrochim Acta A 77:73–81
46. Nowak MJ, Lapinski L, Bienko DC, Michalska D (1997) Infrared matrix isolation spectra of 1-methyluracil—revised assignment based on the Hartree–Fock and post-Hartree–Fock studies. Spectrochim Acta A 53:855–865
47. Mohan S, Sundaraganesan N, Mink J (1991) FTIR and Raman studies on benzimidazole. Spectrochim Acta A 47:1111–1115
48. Palafox MA, Tardajos G, Guerrero-Martínez A, Rastogi VK, Mishra D, Ojha SP, Kiefer W (2007) FT-IR, FT-Raman spectra, density functional computations of the vibrational spectra and molecular geometry of biomolecule 5-aminouracil. Chem Phys 340:17–31
49. Szczesniak M, Nowak MJ, Szczepaniak K, Person WB (1985) Effect of intermolecular interactions on the infrared spectrum of 1-methyluracil. Spectrochim Acta A 41:237–250
50. Singh JS (2008) FTIR and Raman spectra and fundamental frequencies of biomolecule: 5-methyluracil (thymine). J Mol Struct 876:127–133
51. Rastogi VK, Palafox MA, Mittal L, Peica N, Kiefer W, Lang K, Ojha SP (2007) FTIR and FT-Raman spectra and density functional computations of the vibrational spectra, molecular geometry and atomic charges of the biomolecule: 5-bromouracil. J Raman Spectrosc 38:1227–1241